Open access • Journal Article • DOI:10.1109/8.1138

Scattering by a truncated periodic array — Source link

W. L. Ko, Raj Mittra

Institutions: University of Florida

Published on: 01 Apr 1988 - IEEE Transactions on Antennas and Propagation (IEEE)

Topics: Antenna array and Scattering

March 1987 UILU-ENG-87-2217

COORDINATED SCIENCE LABORATORY
College of Engineering

SCATTERING BY A TRUNCATED PERIODIC ARRAY

W. L. Ko
R. Mittra

UNIVERSITY OF ILLINOIS AT URBANA-CHAMPAIGN

UNCLASSIFIED

SECURITY CLASSIFICATION OF THIS PAGE

REPORT DOCUMENTATION PAGE

1a. REPORT SECURITY CLASSIFICATION Unclassified	1b. RESTRICTIVE MARKINGS None
2a. SECURITY CLASSIFICATION AUTHORITY N/A	3. DISTRIBUTION/AVAILABILITY OF REPORT Approved for public release, distribution unlimited.
2b. DECLASSIFICATION/DOWNGRADING SCHEDULE N/A	
4. PERFORMING ORGANIZATION REPORT NUMBER(S) UILU-ENG-87-2217	5. MONITORING ORGANIZATION REPORT NUMBER(S) N/A
6a. NAME OF PERFORMING ORGANIZATION Coordinated Science Laboratory, Univ. of Illinois 6b. OFFICE SYMBOL (If applicable) N/A	7a. NAME OF MONITORING ORGANIZATION Office of Naval Research
6c. ADDRESS (City, State and ZIP Code) 1101 W. Springfield Avenue Urbana, IL 61801	7b. ADDRESS (City, State and ZIP Code) 800 N. Quincy Street Arlington, VA 22217
8a. NAME OF FUNDING/SPONSORING ORGANIZATION Joint Services Electronics Program 8b. OFFICE SYMBOL (If applicable) N/A	9. PROCUREMENT INSTRUMENT IDENTIFICATION NUMBER Contract #N00014-84-C-0149
8c. ADDRESS (City, State and ZIP Code) 800 N. Quincy Street Arlington, VA 22217	10. SOURCE OF FUNDING NOS. PROGRAM ELEMENT NO.: N/A PROJECT NO.: N/A TASK NO.: N/A WORK UNIT NO.: N/A
11. TITLE (Include Security Classification) Scattering by a Truncated Periodic Array	
12. PERSONAL AUTHOR(S) Ko, W. L. and Mittra, R.	
13a. TYPE OF REPORT Technical 13b. TIME COVERED FROM _____ TO _____	14. DATE OF REPORT (Yr., Mo., Day) March 1987 15. PAGE COUNT 51
16. SUPPLEMENTARY NOTATION N/A	
17. COSATI CODES FIELD / GROUP / SUB. GR.	18. SUBJECT TERMS (Continue on reverse if necessary and identify by block number) scattering, frequency selective surface (FSS), truncation, periodic array

19. ABSTRACT (Continue on reverse if necessary and identify by block number)

The scattering characteristics of a doubly periodic array of metallic patches is investigated in this paper from the point of view of detemining the effect of truncating such a screen. The induced surface current on each patch of the array as well as the scattered far-field pattern of the truncated array are computed using the spectral-Galerkin method. The usefulness of the results for the truncated screen problem for the design of frequency selective surfaces (FSS) is discussed.

20. DISTRIBUTION/AVAILABILITY OF ABSTRACT UNCLASSIFIED/UNLIMITED ☒ SAME AS RPT. ☐ DTIC USERS ☐	21. ABSTRACT SECURITY CLASSIFICATION Unclassified
22a. NAME OF RESPONSIBLE INDIVIDUAL	22b. TELEPHONE NUMBER (Include Area Code) 22c. OFFICE SYMBOL None

DD FORM 1473, 83 APR EDITION OF 1 JAN 73 IS OBSOLETE.

UNCLASSIFIED

SECURITY CLASSIFICATION OF THIS PAGE

SCATTERING BY A TRUNCATED PERIODIC ARRAY

W. L. Ko and R. Mittra

ABSTRACT

The scattering characteristics of a doubly periodic array of metallic patches is investigated in this paper from the point of view of determining the effect of truncating such a screen. The induced surface current on each patch of the array as well as the scattered far-field pattern of the truncated array are computed using the spectral-Galerkin method. The usefulness of the results for the truncated screen problem for the design of frequency selective surfaces (FSS) is discussed.

1. INTRODUCTION

In this paper, the problem of scattering by a frequency selective surface (FSS), comprising an array of metallic patches in the x-y plane, is addressed, with the primary objective of investigating the effect of truncation of the FSS on its scattering characteristics. The geometry of the truncated array is shown in Fig. 1. For simplicity of analysis, the screen is truncated in the x- direction only, and it is still infinitely periodic in the y- direction. As is well known, the frequency selective surface finds numerous applications in telecommunications. In the past, this type of array has been treated as an infinite, doubly periodic structure with the resulting simplification that only a single cell of the periodic structure need be considered [1]. However, it is often desirable to assess the edge effects introduced by the truncation of the array. Recently, the finite array problem has been addressed in the literature in the context of patch antennas [2]. In addition, scattering by a finite number of periodic strips has been investigated [3]. In some of these cases, advantage is taken of the long and thin geometry of the structure, comprising strips or dipoles; in others, certain simplifications are employed to make the problem manageable by reducing the number of basis functions for the representation of the current distribution to just one.

In the following sections, we treat the singly truncated periodic array with the spectral-Galerkin method [4], using a set of entire domain basis functions to represent the surface current. The choice of these basis functions is based on the following two criteria: (1) they be analytically Fourier transformable; and, (2) they have the proper edge condition incorporated into their expressions. Section 2 details the analysis of the finite screen problem. Section 3 presents the computed data for the surface current as well as for the

far field. Section 4 discusses the usefulness of this type of structure for frequency selective purposes. Concluding remarks and recommendations for further investigations are found in Section 5.

2. ANALYSIS

For the sake of simplicity, we consider only the case of TM-polarized plane-wave incidence in this work, although the approach applies equally well to the TE case. The array, which is located in the z=0 plane, has a finite number of metallic patches in the x-direction and is infinitely periodic in the y-direction (see Fig. 1). The period in the x-direction is A, and the period in the y-direction is C. The size of the patch is B in the x-direction and D in the y-direction. Since the array is periodic in y, we can solve this problem by considering a single, finite array along the x-axis with appropriate periodic boundary conditions in the y-direction. The problem of scattering is solved in two steps. First, we find the surface current induced on each patch; second, we compute the scattered far-field pattern from the surface currents.

2.1 Computation of Surface Current

To obtain the surface current, we follow the spectral-Galerkin method, which entails the representation of the surface currents in terms of a set of Fourier-transformable basis functions with unknown coefficients. These unknown coefficients are solved for by using the Galerkin method, which generates a system of linear equations by means of a suitably defined inner product that uses the same set of functions for basis as well as testing. It is well known that by Fourier transforming a set of equations involving differential and integral operators, a set of algebraic equations involving only multiplications and divisions can be obtained. To take advantage of this fact, Galerkin's method of analysis is carried out in the Fourier transform or the spectral domain; hence, the name spectral-Galerkin method.

An alternative approach to solving this problem would be to use an iterative approach, e.g., the conjugate-gradient method, which has found extensive

application to the infinite FSS problem [5]. Recently, an attempt has also been made to apply the iterative procedure to the solution of the truncated FSS problem [6]. However, it has been found that the iterative procedure is fraught with difficulties associated with convergence and accuracy, due primarily to a very large number of unknowns required to adequately describe the finite FSS problem using a FFT-based iteration procedure.

Returning to the spectral-Galerkin procedure, the first step is to write the integral equation for the surface current in the transform domain. The Fourier transform $\tilde{\bar{J}}$ of the surface current $\bar{J}(x,y)=\hat{x}J_x(x,y)+\hat{y}J_y(x,y)$ satisfies the equation

$$\tilde{\bar{\bar{G}}} \cdot \tilde{\bar{J}} = j \frac{k}{z_o} \sum_{\ell} (-\tilde{E}_x^{i,\ell}) \tag{1}$$

in which

$$\tilde{\bar{\bar{G}}} = \begin{bmatrix} \tilde{G}_{xx} & \tilde{G}_{xy} \\ \tilde{G}_{yx} & \tilde{G}_{yy} \end{bmatrix} = \begin{bmatrix} k^2 - \alpha^2 & -\alpha\beta \\ -\alpha\beta & k^2 - \beta^2 \end{bmatrix} \frac{1}{2\gamma} \tag{2}$$

and

$$\gamma = \begin{cases} -j\sqrt{k^2 - \alpha^2 - \beta^2} & \text{if } k > (\alpha^2 + \beta^2) \\ -\sqrt{\alpha^2 + \beta^2 - k^2} & \text{if } k < (\alpha^2 + \beta^2) \end{cases} \tag{3}$$

The symbol ~ on top of a quantity designates the Fourier transform of that quantity. The conventions of $\exp(j\omega t)$ and $\exp(\gamma z)$ are used in this paper. The Fourier transform pair, as employed herein, is defined as

$$\tilde{F}(\alpha,\beta) = \int_{-\infty}^{\infty}\int F(x,y)\exp[-j(\alpha x + \beta y)]\,dxdy$$

$$F(x,y) = \frac{1}{(2\pi)^2}\int_{-\infty}^{\infty}\int \tilde{F}(\alpha,\beta)\exp[j(\alpha x + \beta y)]\,d\alpha d\beta \tag{4}$$

The right-hand side of (1) contains the summation of the Fourier transform of the incident field $E_x^{i,\ell}$ on the individual patches. The boundary condition that the tangential E-field vanish on the patches has been used in writing (1).

Consider the current on the ℓ-th patch:

$$\overline{J}^{\ell} = \hat{x}\, J_x^{\ell} + \hat{y}\, J_y^{\ell} \tag{5}$$

where

$$J_x^{\ell} = \sum_{r,s} d_{rs}^{\ell}\ \phi_{x,rs}^{\ell} \tag{6}$$

$$J_y^{\ell} = \sum_{p,q} c_{pq}^{\ell}\ \phi_{y,pq}^{\ell} \tag{7}$$

and d_{rs}^{ℓ} and c_{pq}^{ℓ} are unknown coefficients. The basis functions $\phi_{x,rs}^{\ell}$ and $\phi_{y,pq}^{\ell}$ are chosen such that they incorporate the correct singularities for the current at the edges of the patch. These basis functions can be written as

$$\phi_{x,rs}^{\ell} = \sin\left\{\frac{r\pi}{B}\left[(x - \ell A) + \frac{B}{2}\right]\right\}\frac{T_s\left(\frac{2}{D}y\right)}{\left[1-\left(\frac{2}{D}y\right)^2\right]^{1/2}} \tag{8}$$

where

$$r = 1, 2, \ldots, IRR \tag{8a}$$

$$s = 0, 1, \ldots, ISS-1 \tag{8b}$$

$$\ell = -\left(\frac{N-1}{2}\right), \ldots, 0, \ldots, \left(\frac{N-1}{2}\right) \tag{8c}$$

and
$$\phi^{\ell}_{y,pq} = \frac{T_p\left[\frac{2}{B}(x-\ell A)\right]}{\left\{1-\left[\frac{2}{B}(x-\ell A)\right]^2\right\}^{1/2}} \sin\left[\frac{q\pi}{D}\left(y+\frac{D}{2}\right)\right] \tag{9}$$

where
$$p = 0, 1, \ldots, IPP-1 \tag{9a}$$
$$q = 1, 2, \ldots, IQQ \tag{9b}$$

The T_i in (9) is the i-th order Chebyshev polynomial of the first kind. There are a total of N patches. The index ℓ designates the ℓ-th patch, and it is computed according to (8c). The number of basis functions in the x- direction is given by (IRR x ISS) and in the y- direction (IPP x IQQ). Note that the running indices r and q start from 1 and the running indices p and s start from 0. The basis functions given in (8) and (9) are then Fourier transformed to obtain $\tilde{J}$, whose x- and y-components are given by

$$\tilde{J}^{\ell}_x = \sum_{r,s} D^{\ell}_{rs}\, \tilde{\phi}^{\ell}_{x,rs} \tag{10}$$

$$\tilde{J}^{\ell}_y = \sum_{p,q} C^{\ell}_{pq}\, \tilde{\phi}^{\ell}_{y,pq} \tag{11}$$

where
$$D^{\ell}_{rs} = d^{\ell}_{rs}\, C''_{rs} \tag{12}$$
$$C^{\ell}_{pq} = c^{\ell}_{pq}\, C'_{pq} \tag{13}$$

The quantities d^{ℓ}_{rs} and c^{ℓ}_{pq} are defined in (6) and (7). From (6), (7), (10), (11), and (4), we can write

$$C''_{rs}\, \tilde{\phi}^{\ell}_{x,rs} = \int_{-\infty}^{\infty}\int \phi^{\ell}_{x,rs}(x,y)\, \exp[-j(\alpha x + \beta y)]\, dxdy \tag{14}$$

$$C'_{pq}\,\tilde{\phi}^{\ell}_{y,pq} = \int_{-\infty}^{\infty}\int \phi^{\ell}_{y,pq}(x,y)\,\exp[-j(\alpha x + \beta y)]\,dxdy \tag{15}$$

Substituting (8) and (9) into (14) and (15), we obtain

$$\tilde{\phi}^{\ell}_{x,rs} = \left[\left[\mathrm{sinc}\left(\frac{r\pi}{2} - \frac{\beta\alpha}{2}\right) + (-1)^{r-1}\mathrm{sinc}\left(\frac{r\pi}{2} + \frac{\beta\alpha}{2}\right)\right]\right.$$

$$\left.\cdot\,\exp[-j\,\alpha\,(\ell A)]\right] \cdot J_s\left(\frac{D}{2}\beta\right) \tag{16}$$

$$C''_{rs} = \frac{B}{2}\,j^{(r-1)}\,\frac{D}{2}\,(-j)^{s}\pi \tag{17}$$

$$\tilde{\phi}^{\ell}_{y,pq} = J_p\left(\frac{B}{2}\,\alpha\right)\exp[-j\alpha(\ell A)]$$

$$\cdot\left[\mathrm{sinc}\left(\frac{q\pi}{2} - \frac{D}{2}\,\beta\right) + (-1)^{q-1}\mathrm{sinc}\left(\frac{q\pi}{2} + \frac{D}{2}\,\beta\right)\right] \tag{18}$$

$$C'_{pq} = \frac{B}{2}\,(-j)^{P}\,\pi\,\frac{D}{2}\,j^{(q-1)} \tag{19}$$

In the above equations, sinc(.)=sin(.)/(.) and J_i is the i-th order Bessel function of the first kind.

With all of the quantities defined above, we can write (1) in its x- and y-components as

$$\bar{\bar{G}} \cdot \bar{J} = \hat{x}\,(\bar{\bar{G}} \cdot \bar{J})_x + \hat{y}\,(\bar{\bar{G}} \cdot \bar{J})_y$$

$$= \hat{x}\,(\tilde{G}_{xx}\,\tilde{J}_x + \tilde{G}_{xy}\,\tilde{J}_y) + \hat{y}\,(\tilde{G}_{yx}\,\tilde{J}_x + \tilde{G}_{yy}\,\tilde{J}_y)$$

$$= \hat{x}\,j\,\frac{k}{z_o}\sum_{\ell}\,(-\tilde{E}^{\,i,\ell}_{x}) + \hat{y}\,(0) \tag{20}$$

Defining an inner product

$$\langle \bar{A} \cdot \bar{B} \rangle \triangleq \int_{-\infty}^{\infty}\int \bar{A} \cdot \bar{B}^{*} \, d\alpha d\beta \tag{21}$$

and applying the spectral-Galerkin method to (20), we obtain the following (L x R x S) x-component equations:

$$\sum_{rs} D_{rs}^{\ell *} \int_{-\infty}^{\infty}\int \tilde{\phi}_{x,RS}^{L} \tilde{G}_{xx}^{*} \tilde{\phi}_{x,rs}^{\ell *} \, d\alpha d\beta$$

$$+ \sum_{pq} C_{pq}^{\ell *} \int_{-\infty}^{\infty}\int \tilde{\phi}_{x,RS}^{L} \tilde{G}_{xy}^{*} \tilde{\phi}_{y,pq}^{\ell *} \, d\alpha d\beta$$

$$= \int_{-\infty}^{\infty}\int \tilde{\phi}_{x,RS}^{L} \left[-j \frac{k}{z_o} \sum_{\ell} (-\tilde{E}_{x}^{i,\ell *})\right] d\alpha d\beta \tag{22}$$

and the following (L x P x Q) y-component equations:

$$\sum_{rs} D_{rs}^{\ell *} \int_{-\infty}^{\infty}\int \tilde{\phi}_{y,PQ}^{L} \tilde{G}_{yx}^{*} \tilde{\phi}_{x,rs}^{\ell *} \, d\alpha d\beta$$

$$+ \sum_{pq} C_{pq}^{\ell *} \int_{-\infty}^{\infty}\int \tilde{\phi}_{y,PQ}^{L} \tilde{G}_{yy}^{*} \tilde{\phi}_{y,pq}^{\ell *} \, d\alpha d\beta$$

$$= 0 \tag{23}$$

The above equations can be rearranged into a matrix form:

$$\begin{array}{l} \\ \text{LRS rows} \\ \text{LPQ rows} \end{array} \overbrace{\begin{array}{|c|c|} \hline \langle \text{LRS}, \ell pq \rangle & \langle \text{LRS}, \ell rs \rangle \\ \hline \langle \text{LPQ}, \ell pq \rangle & \langle \text{LPQ}, \ell rs \rangle \\ \hline \end{array}}^{\begin{array}{c}\ell pq \text{ columns} \\ \end{array} \quad \overbrace{\phantom{\langle \text{LRS}, \ell rs \rangle}}^{\ell rs \text{ columns}}} \begin{bmatrix} C_{pq}^{\ell *} \\ \hline D_{rs}^{\ell *} \end{bmatrix} \begin{array}{l} \} \ \ell pq \text{ unknowns} \\ \} \ \ell rs \text{ unknowns} \end{array} = \begin{array}{l} \\ \} \ \text{LRS rows} \\ \} \ \text{LPQ rows} \end{array} \begin{bmatrix} \langle \text{LRS}, \sum_{\ell} \tilde{-E}^{i}, \ell_{x} \rangle \\ \hline 0 \end{bmatrix} \tag{24}$$

where the matrix elements are given as

$$\langle \text{LRS}, \ell pq \rangle$$

$$= \int_{-\infty}^{\infty} \tilde{\phi}_{x,RS}^{L} \ \tilde{G}_{xy}^{*} \ \tilde{\phi}_{y,pq}^{\ell *} \, d\alpha d\beta$$

$$= \sum_{n} \int_{-\infty}^{\infty} \{[\text{sinc}\,(\tfrac{R\pi}{2} - \tfrac{B}{2}\alpha) + (-1)^{R-1} \text{ sinc}\,(\tfrac{R\pi}{2} + \tfrac{B}{2}\alpha)]$$

$$\cdot \exp(-j\,\alpha\,LA) \cdot J_S\,(\tfrac{D}{2}\beta_n) \cdot (-\alpha\beta_n) \cdot [\tfrac{1}{2\gamma(\alpha,\beta_n)}]^{*}$$

$$\cdot J_p\,(\tfrac{B}{2}\alpha) \exp(j\,\alpha\,\ell\,A)[\text{sinc}(\tfrac{q\pi}{2} - \tfrac{D}{2}\beta_n)$$

$$+ (-1)^{q-1} \text{ sinc}\,(\tfrac{q\pi}{2} + \tfrac{D}{2}\beta_n)]\} \, d\alpha \tag{25}$$

$$< \text{LPQ}, \ell rs > = \int_{-\infty}^{\infty}\int \tilde{\phi}^{L}_{y,PQ}\ \tilde{G}^{*}_{yx}\ \tilde{\phi}^{\ell *}_{x,rs}\ d\alpha d\beta$$

$$= \sum_{n} \int_{-\infty}^{\infty} \{ J_p\ (\tfrac{B}{2}\alpha)\ \exp(-j\ \alpha\ LA)$$

$$\cdot\ [\operatorname{sinc}(\tfrac{Q\pi}{2} - \tfrac{D}{2}\beta_n) + (-1)^{Q-1}\operatorname{sinc}(\tfrac{Q\pi}{2} + \tfrac{D}{2}\beta_n)]$$

$$\cdot\ (-\alpha\ \beta_n)\ [\frac{1}{2\gamma(\alpha,\beta_n)}]^{*}$$

$$\cdot\ [\operatorname{sinc}(\tfrac{r\pi}{2} - \tfrac{B}{2}\alpha) + (-1)^{r-1}\ \operatorname{sinc}(\tfrac{r\pi}{2} + \tfrac{B}{2}\alpha)]$$

$$\cdot\ \exp(j\ \alpha\ \ell\ A) \cdot J_s\ (\tfrac{D}{2}\beta_n)\}\ d\alpha \qquad (26)$$

$$< \text{LRS}, \ell rs > = \int_{-\infty}^{\infty}\int \tilde{\phi}^{L}_{x,RS}\ \tilde{G}^{*}_{xx}\ \tilde{\phi}^{\ell *}_{x,rs}\ d\alpha d\beta$$

$$= \sum_{n} \int_{-\infty}^{\infty} [\operatorname{sinc}(\tfrac{R\pi}{2} - \tfrac{B}{2}\alpha) + (-1)^{R-1}\operatorname{sinc}(\tfrac{R\pi}{2} + \tfrac{B}{2}\alpha)]$$

$$\cdot\ \exp(-j\ \alpha\ LA) \cdot J_S\ (\tfrac{D}{2}\beta_n) \cdot (k^2 - \alpha^2)[\frac{1}{2\gamma(\alpha,\beta_n)}]^{*}$$

$$\cdot\ [\operatorname{sinc}(\tfrac{r\pi}{2} - \tfrac{B\alpha}{2}) + (-1)^{r-1}\operatorname{sinc}(\tfrac{r\pi}{2} + \tfrac{B}{2}\alpha)]$$

$$\cdot\ \exp(j\ \alpha\ \ell A) \cdot J_s\ (\tfrac{D}{2}\beta_n)\}\ d\alpha \qquad (27)$$

$$< \mathrm{LPQ},\ \ell pq > = \int_{-\infty}^{\infty} \tilde{\phi}^{L}_{y,PQ}\ \tilde{G}^{*}_{yy}\ \ \tilde{\phi}^{\ell *}_{y,pq}\ d\alpha d\beta$$

$$= \sum_{n} \int_{-\infty}^{\infty} \{[J_p\ (\tfrac{B}{2}\alpha)\ \exp(-j\ \alpha\ LA)$$

$$\cdot\ \mathrm{sinc}\ (\tfrac{Q\pi}{2} - \tfrac{D}{2}\beta_n) + (-1)^{Q-1}\mathrm{sinc}(\tfrac{Q\pi}{2} + \tfrac{D}{2}\beta_n)]$$

$$\cdot\ (k^2 - \beta_n^2)\ [\frac{1}{2\gamma(\alpha,\beta_n)}]^{*}$$

$$\cdot\ J_p\ (\tfrac{B}{2}\alpha)\ \exp(j\ \alpha\ \ell\ A)$$

$$\cdot\ \mathrm{sinc}\ (\tfrac{q\pi}{2} - \tfrac{D}{2}\beta_n) + (-1)^{q-1}\mathrm{sinc}(\tfrac{q\pi}{2} + \tfrac{D}{2}\beta_n)\}\ d\alpha \qquad (28)$$

The first half of the right-hand side in (24) is given by

$$< \mathrm{LRS},\ \sum_{\ell} - \tilde{E}^{i,\ell}_{x} >$$

$$= \int_{-\infty}^{\infty} \tilde{\phi}^{L}_{x,RS}\ [-j\ \frac{k}{z_o} \sum_{\ell} (-\tilde{E}^{i,\ell^*}_{x})]\ d\alpha d\beta$$

$$= \sum_{\ell} \sum_{n} \int_{-\infty}^{\infty} [\mathrm{sinc}(\tfrac{R\pi}{2} - \tfrac{B\alpha}{2}) + (-1)^{R-1}\mathrm{sinc}(\tfrac{R\pi}{2} + \tfrac{B}{2}\alpha)]$$

$$\cdot\ \exp(-j\ \alpha\ LA)\ \cdot\ J_S\ (\tfrac{D}{2}\beta_n)\ (-j\ \frac{k}{z_o})\ (-\cos\theta_i)$$

$$\cdot\ \exp[j(\alpha - \alpha_o)\ \ell A]\ \cdot\ D\ \cdot\ B\ \cdot\ \mathrm{sinc}[(\alpha - \alpha_o)\tfrac{B}{2}]$$

$$\cdot\ \mathrm{sinc}\ (\beta_n\ \tfrac{D}{2})\ d\alpha \qquad (29)$$

where

$$\alpha_o = k \sin \theta_i$$

k is the wave number, and

θ_i is the incident angle.

The second half of the right-hand side is equal to zero because of the assumed polarization of the incident field in this study. It can be readily modified to handle other polarizations as well.

Because the array is infinitely periodic in y, we can sample the corresponding transformed variable β according to Floquet's theorem. In the present case, where incidence is parallel to the $\theta_i = 0$ plane, we have

$$\beta_n = \frac{2\pi n}{C} \quad , n=0, \pm 1, \pm 2, \ldots \tag{30}$$

where C is the spatial period in the y-direction. On the other hand, since the periodic array is truncated along x, the number of patches along the x-direction is finite. Therefore, we integrate along this direction over the finite length of the array. The integration can be performed conveniently by using the fast Fourier transform (FFT) algorithm. Notice that the integrals in (25), (26), (27), (28), and (29) are of the following generic form

$$\int_{-\infty}^{\infty} f(\alpha,\beta_n) \exp\{j[(\ell-L)A]\alpha\}\, d\alpha \tag{31}$$

Therefore, only one FFT of the function $f(\alpha,\beta_n)$ is needed to compute the above integral for various combinations of the indices ℓ and L, whose values are given in (8c). In other words, we choose the FFT samples where $x = (\ell - L)\, A$. After all of the entries in the matrix and the right-hand side in (24) have been computed, we can solve for the unknown coefficients C's and D's by standard

methods available for the solution of simultaneous algebraic equations. For example, Cholesky's method is used to generate results in this paper. The C's and D's are then substituted into (12) and (13) and the c's and d's are computed. These are, in turn, substituted into (6) and (7) to evaluate the surface current on each patch. Numerical results based on this procedure are presented in Section 3.

2.2 Computation of Scattered Far Field

To complete the scattering analysis, we compute the scattered far field from the induced surface currents on the patches. In the $\phi = \pi$ half-plane, we desire to compute the θ- and ϕ- components of the far E-field, viz., E_θ and E_ϕ, for θ between 0 and 90 degrees. It is found [7] that $|E_\theta| \alpha |N_\theta|$ and $|E_\phi| \alpha |N_\phi|$, where

$$N_\theta = -\cos\theta \int\int_{\text{All patches}} J_x \exp[-j(k \sin\theta)x]\, dxdy \tag{32}$$

and

$$N_\phi = -\int\int_{\text{All patches}} J_y \exp[-j(k \sin\theta)x]\, dxdy \tag{33}$$

Using (4),(6),(7),(10), and (11), we can rewrite the above two equations in the following manner:

$$N_\theta = -\cos\theta \sum_\ell \tilde{J}_x^\ell \ (\alpha = k \sin\theta,\ \beta = 0) \tag{34}$$

and

$$N_\phi = -\sum_\ell \tilde{J}_y^\ell \ (\alpha = k \sin\theta,\ \beta = 0) \tag{35}$$

It is now seen that the far field can be computed readily by a weighted summation of the transformed basis functions evaluated at $\alpha = k \sin\theta$ and $\beta = 0$. The weights of the terms in the above summation are simply the appropriate coefficients C's and D's given in (12) and (13). Thus, we can write

$$|E_\theta| \propto \left| -\cos\theta \sum_{\ell} \sum_{r} \sum_{s} D^{\ell}_{rs} \tilde{\phi}^{\ell}_{x,rs} (\alpha = k \sin\theta, \beta = 0) \right| \qquad (36)$$

and

$$|E_\phi| \propto \left| -\sum_{\ell} \sum_{p} \sum_{q} C^{\ell}_{pq} \tilde{\phi}^{\ell}_{y,pq} (\alpha = k \sin\theta, \beta = 0) \right| \qquad (37)$$

The far-field patterns computed using the above equations are presented in the next section along with the surface current distributions.

3. NUMERICAL RESULTS

In this section, we present the results for the surface currents and the far-field patterns of a truncated FSS screen computed at various frequencies.

3.1 Surface Current

The x- and y-components of the surface current normalized to the incident H-field, i.e., J_x/H and J_y/H, have been computed along the center line of each patch in the x- and y- directions, with the exception of J_y/H vs. x, which has been plotted for $y = -d/4$, since it is essentially negligible along the center line (i.e. $y = 0$). The x- and y-dimensions of the plot have been normalized to the respective cell sizes in these dimensions. Figures 2,3,4,5, and 6 show the surface currents of a 9-patch array illuminated by a TM-polarized plane wave incident from θ^i =45 degrees, and $\phi^i = 0°$, for five frequencies, viz., 3, 15, 24, 36, and 45 GHz. These currents have been computed using sixteen basis functions (4 in x and 4 in y) to ensure convergence, although typically 9 basis functions are found to be adequate. The corresponding results for the surface currents of a 5- and a 3-patch array are shown in Figs. 7 and 8, respectively, for the frequency of 24 GHz. Note that the starting frequency of computation is well below the resonant frequency of the FSS, which occurs at around 24 GHz, whereas the highest frequency of computation is well above the resonance. This allows us to investigate the out-of-band performance of the FSS.

3.2 Far-Field Patterns

The co-polarized and the cross-polarized far-field components, E_θ and E_ϕ, are displayed in Figs. 10, 11, 12, 13, and 14 for the 9-patch array illuminated by a TM-polarized plane wave incident from $\theta^i = 45$ degrees and $\phi^i = 0$, for five frequencies spanning the range 3 to 45 GHz. The corresponding surface currents of these patterns were shown in Figs. 2, 3, 4, 5, and 6. Figures 15

and 16 display the corresponding patterns for a 5- and a 3-patch array, respectively. Finally, the pattern of a 3-patch array with normal incidence is shown in Fig. 17.

A discussion of the above results is presented in the following section.

4. SCATTERING CHARACTERISTICS

From the computed data presented in the previous section, we can observe that the array scatters strongly in the specular direction with a well-defined main beam of the scattered field pointing in this direction. As expected, the frequency selective array shows a strong dependency on the frequency of the incident plane wave. For example, the magnitude of the patch currents at 3 GHz, which is well below the resonant frequency, and the corresponding radiated field are negligible compared with their counterparts at higher frequencies. The frequency selective property of the screen is evident from the behavior of the currents and the far field at the other frequencies. Parametric investigation of these characteristics enables one to design the FSS screen to meet the desired specifications.

Another important observation is that the surface currents are almost identical for all of the patches in the array except for those near the truncated edges of the array. This edge effect is clearly noticeable from the computed data and leads one to conclude that the simple approximation based on the assumption that the perturbation from the doubly infinite periodic case is negligible is not a good one. However, since the modification of the surface current is seen to be confined to the edge patches only, it appears reasonable to assume that for the finite, rectangular patch FSS problem, all of the inner patches have the same current distribution as that existing on the center patch and extend the size of the array in the finite dimension to a very large number, without significantly increasing the number of unknowns to be solved for in the application of the spectral- Galerkin method.

5.CONCLUSIONS

In this paper, we have solved the problem of scattering by a truncated periodic planar array of metallic rectangular patches with TM-polarized plane-wave illumination at an oblique incidence angle. Since the array is infinitely periodic in one dimension and finitely periodic in the other, the problem can be solved by considering one row of patches in the finite dimension. Therefore, it is equivalent to treating the problem of scattering by a linear array of a finite number of patches. The induced surface currents on the patches have been computed using the spectral-Galerkin method. The scattered far-field pattern of the finite array has also been obtained.

The important findings of this work are summarized as follows: (1) The edge effect is clearly observable and should not be ignored; (2) The array scatters strongly in the specular reflection direction; and, (3) This type of surface scatters with a strong dependency on the frequency of the incident wave and, hence, can be used as a frequency selective surface.

Because the truncated screen problem requires a rather large number of unknowns to derive an accurate solution, the computation can be quite time consuming. It takes about 2 hours of CPU time (about 4 hours of elapsed time) on a VAX-8600 to generate a set of data at a single frequency for a 9-patch array with (4 x 4) basis functions along each dimension. Although not discussed here, recent efforts have been successfully directed toward reducing this computation time by increasing the efficiency of the computation of the matrix element. Additional insight gained from the present work is helpful in formulating other approaches by which the computer time and storage problems could be alleviated even further. One could attack the large finite array problems without ignoring the edge effects by assuming that the inner patches have identical current

distributions as the center patch and by treating the currents on the edge patches and possibly on one or two inside patches next to the edge patches as unknowns in the spectral-Galerkin's method. In this manner, we can increase the number of patches in the finite array without increasing the number of unknowns. We also plan to extend this work to a conformal FSS printed on a cylindrical surface, by using an approach similar to what has been described in this paper for planar arrays. The curved array is inherently more complicated because for each patch on the curved surface, the incident angle of the plane-wave illumination may look different.

REFERENCES

[1] C.C. Chen, "Scattering by a two-dimensional periodic array of conducting plates," IEEE Trans. Antennas Propagat., vol. AP-18, pp. 660-665, September 1970.

[2] D.M. Pozar, "Finite phased arrays of rectangular microstrip patches," IEEE Trans. Antennas Propagat., vol. AP-34, pp.658- 665, May 1986.

[3] T. Cwik and R. Mittra, "The effects of the truncation and curvature of periodic surfaces: A strip grating," to be published in AP-S.

[4] C. H. Tsao and R. Mittra, "Spectral-domain analysis of frequency selective surfaces comprised of periodic arrays of cross dipoles and Jerusalem crosses," IEEE Trans. on Antennas and Propagation, vol. AP-32, no. 5, pp. 478-486, May 1984.

[5] T. Cwik and R. Mittra, "Scattering from general periodic screens," Electromagnetics, vol. 5, no. 4, pp. 263-283, 1985.

[6] R. Kastner and R. Mittra, "Iterative analysis of finite-sized planar frequency selective surfaces with rectangular patches or perforations," submitted to AP-S.

[7] C.A. Balanis, Antenna Theory Analysis and Design, New York: Harper & Row, 1982.

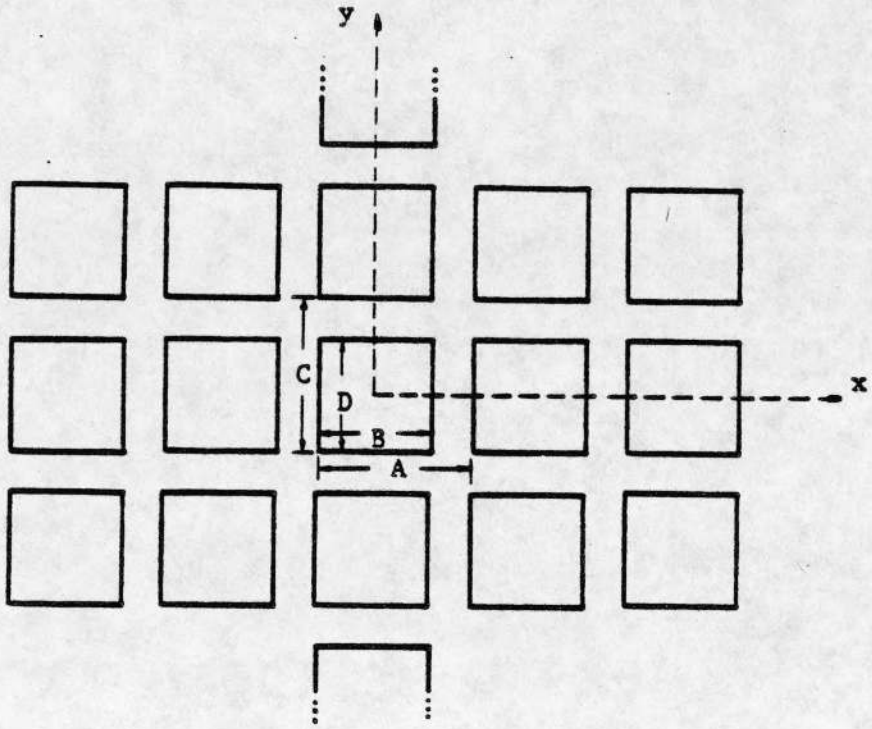

Figure 1. Geometry of a finite FSS array, periodic in y and truncated in x-direction.

Figure 2. Current distribution on 9 patch finite FSS (A = 1 cm, C = 1 cm, B = 0.8 cm, D = 0.8 cm) for $\theta^I = 45°$ and $\phi^I = 0°$ and TM polarization. Frequency f = 3 GHz.

(a) $J_y/|H^i|$ vs. x sampled at y = -d/4, and $J_y/|H^i|$ vs. y sampled at center line of each patch.

(b) $J_x/|H^i|$ vs. x and y sampled at center lines of each patch in the horizonal and vertical directions.

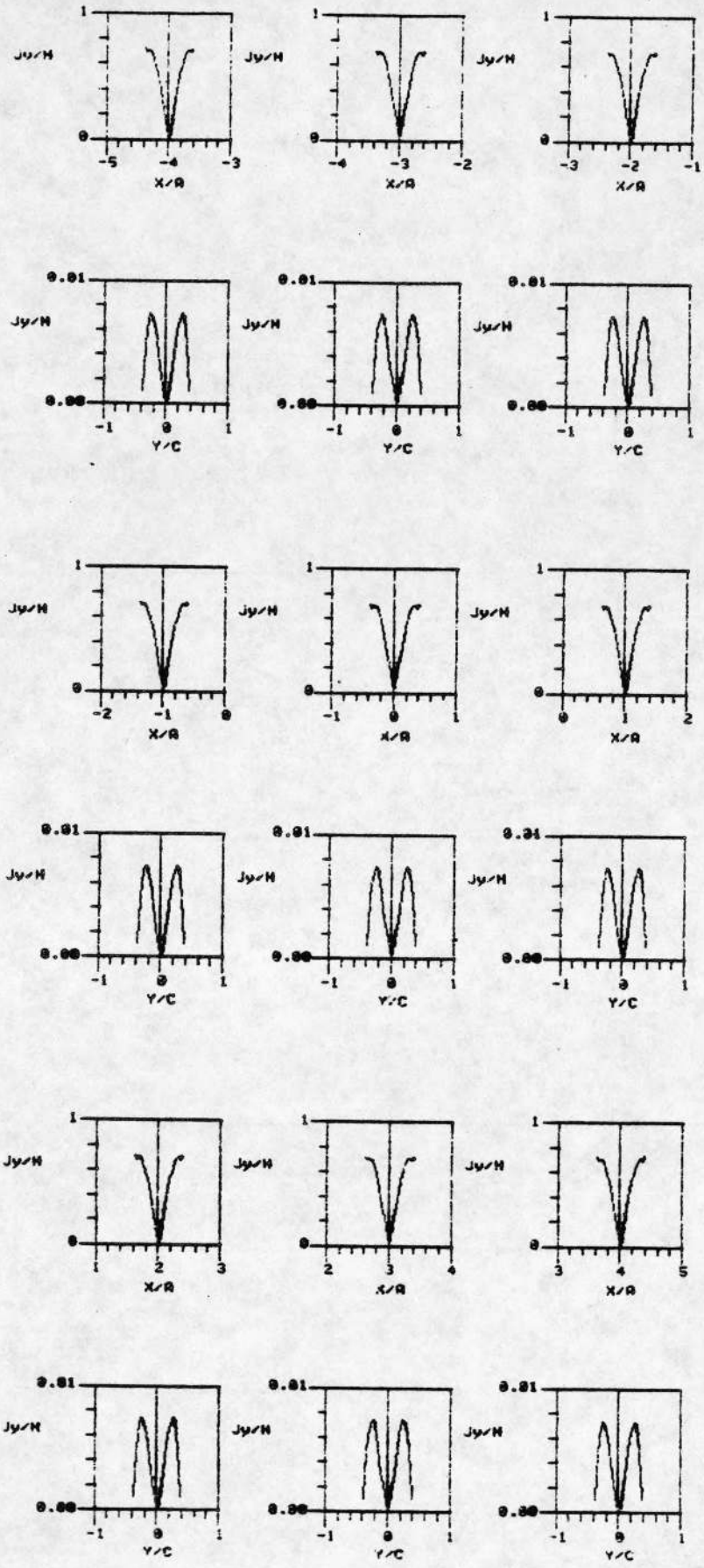

Figure 2(a)

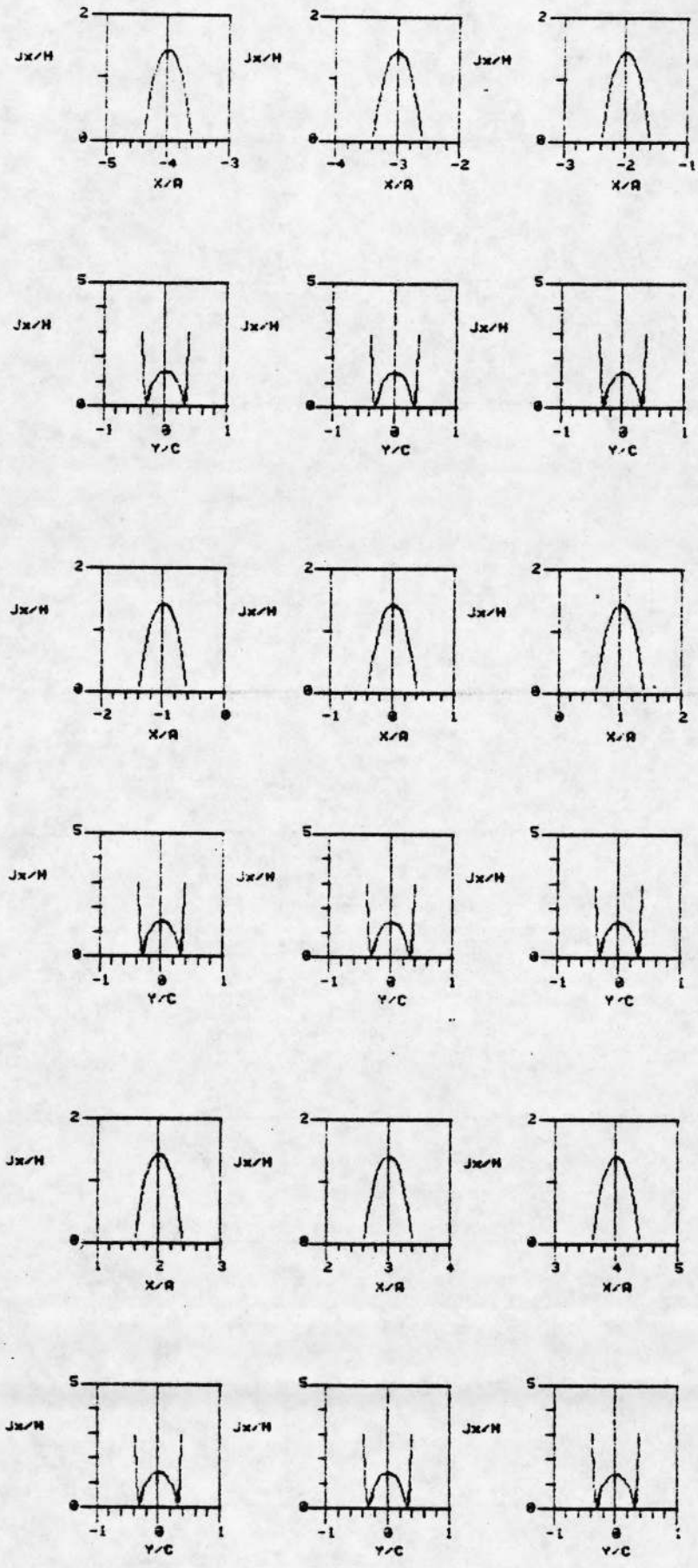

Figure 2(b)

Figure 3. Current distribution on 9 patch finite FSS (A = 1 cm, C = 1 cm, B = 0.8 cm, D = 0.8 cm) for $\theta^i = 45°$ and $\phi^i = 0°$ and TM polarization. Frequency f = 15 GHz.

(a) $J_y/|H^i|$ vs. x sampled at y = -d/4, and $J_y/|H^i|$ vs. y sampled at center line of each patch.

(b) $J_x/|H^i|$ vs. x and y sampled at center lines of each patch in the horizonal and vertical directions.

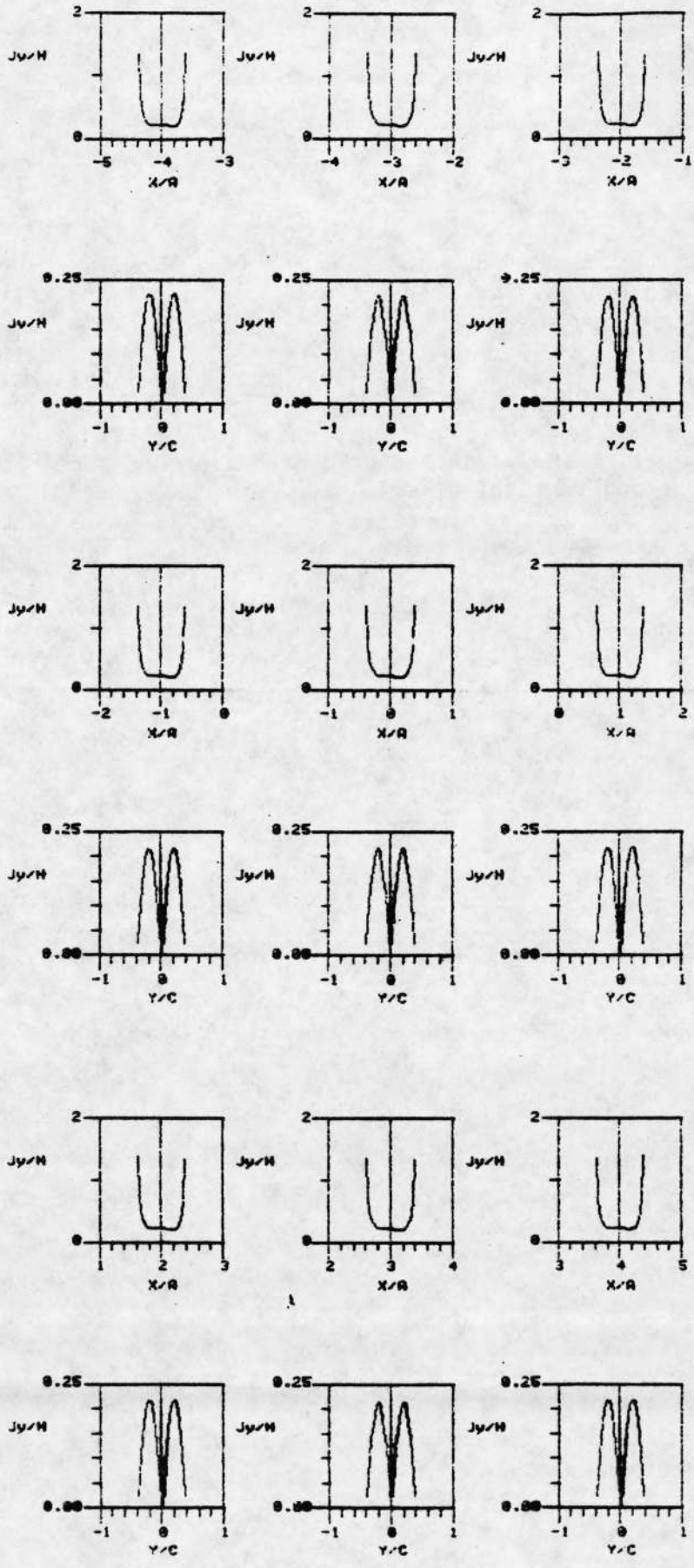

Figure 3(a)

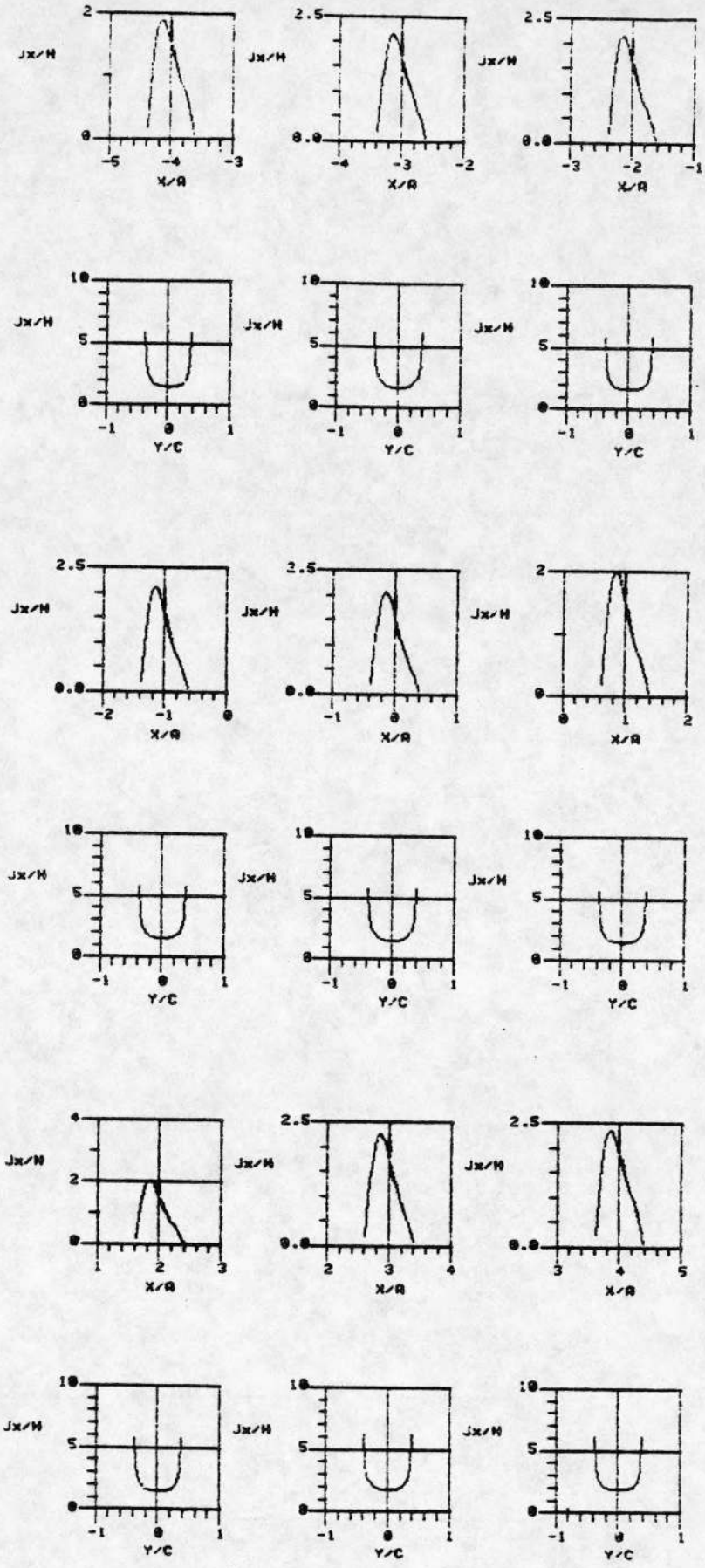

Figure 3(b)

Figure 4. Current distribution on 9 patch finite FSS (A = 1 cm, C = 1 cm, B = 0.8 cm, D = 0.8 cm) for $\theta^i = 45°$ and $\phi^i = 0°$ and TM polarization. Frequency f = 24 GHz.

(a) $J_y/|H^i|$ vs. x sampled at y = -d/4, and $J_y/|H^i|$ vs. y sampled at center line of each patch.

(b) $J_x/|H^i|$ vs. x and y sampled at center lines of each patch in the horizonal and vertical directions.

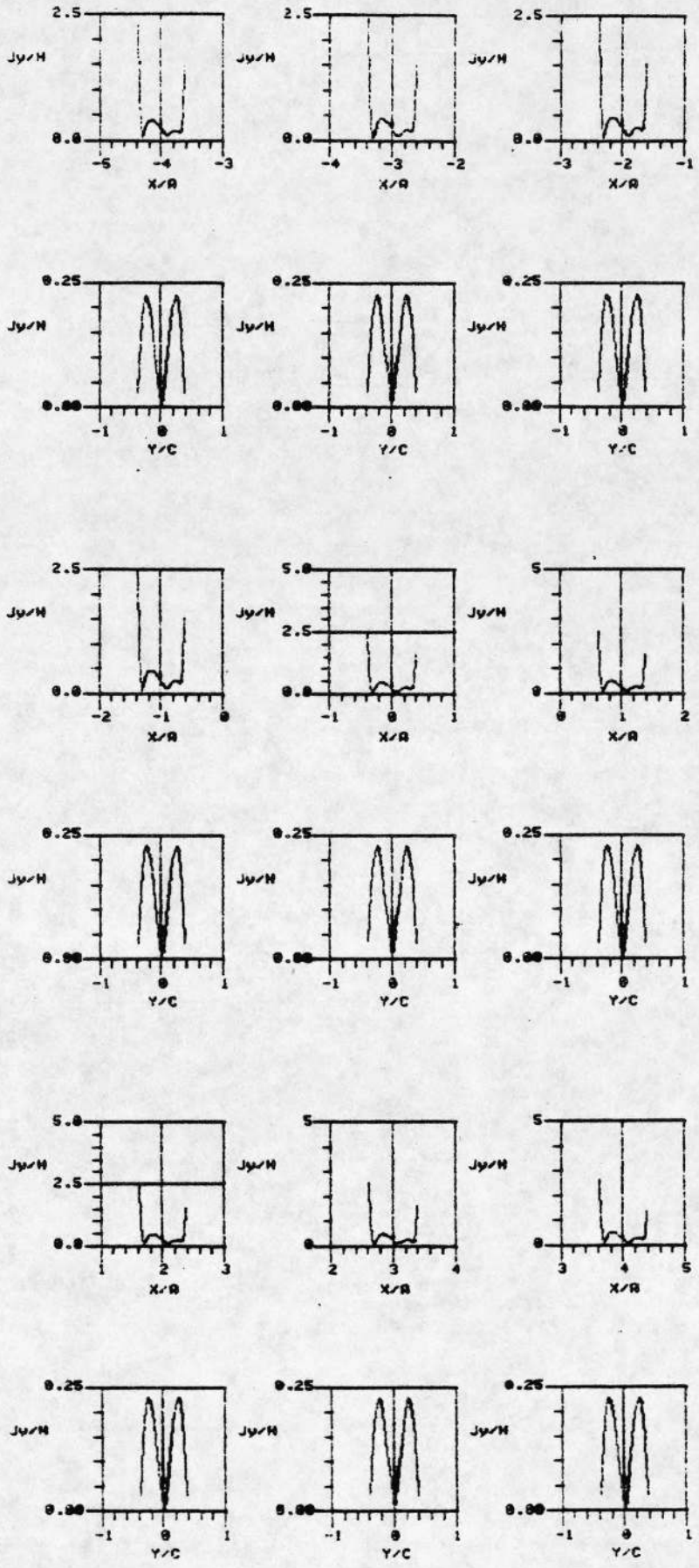

Figure 4(a)

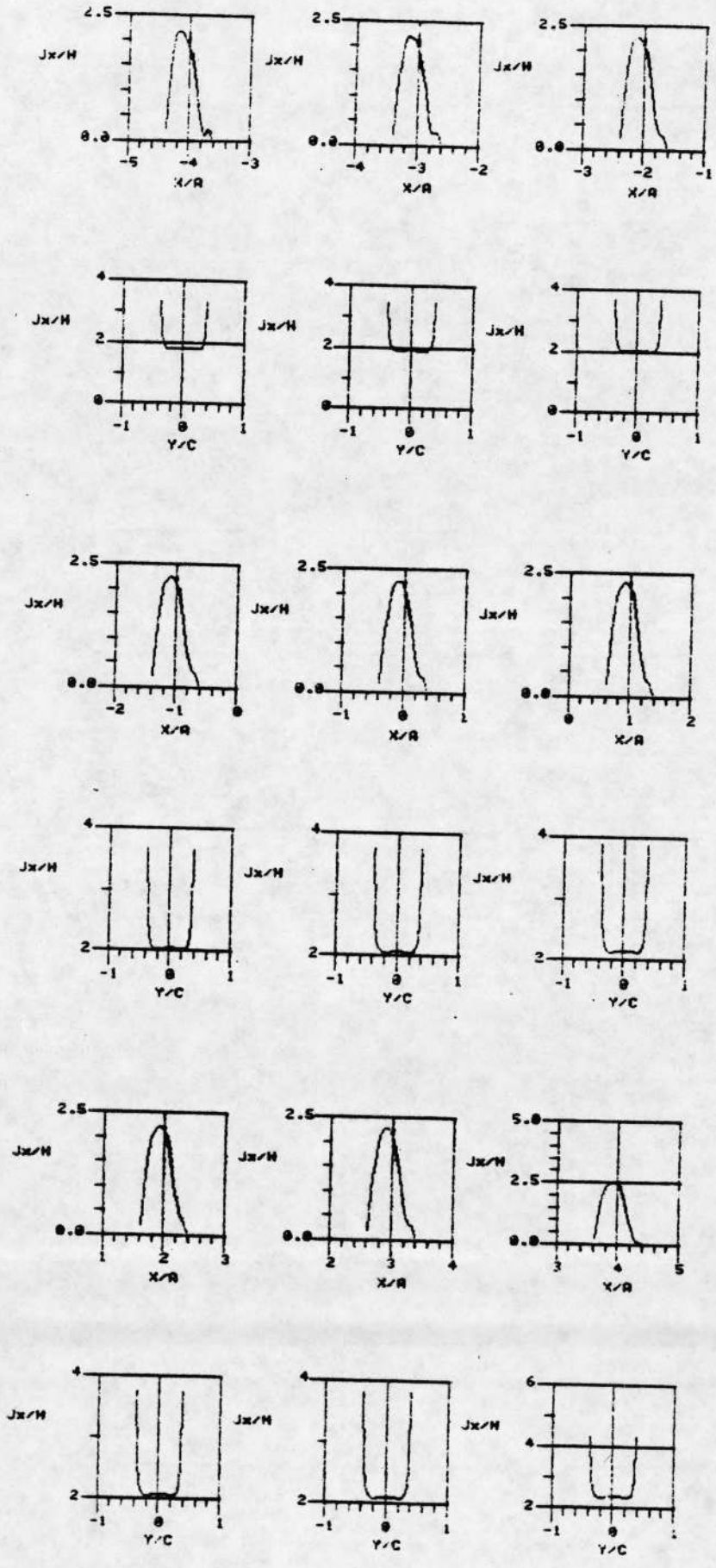

Figure 4(b)

Figure 5. Current distribution on 9 patch finite FSS (A = 1 cm, C = 1 cm, B = 0.8 cm, D = 0.8 cm) for $\theta^i = 45°$ and $\phi^i = 0°$ and TM polarization. Frequency f = 36 GHz.

(a) $J_y/|H^i|$ vs. x sampled at y = -d/4, and $J_y/|H^i|$ vs. y sampled at center line of each patch.

(b) $J_x/|H^i|$ vs. x and y sampled at center lines of each patch in the horizonal and vertical directions.

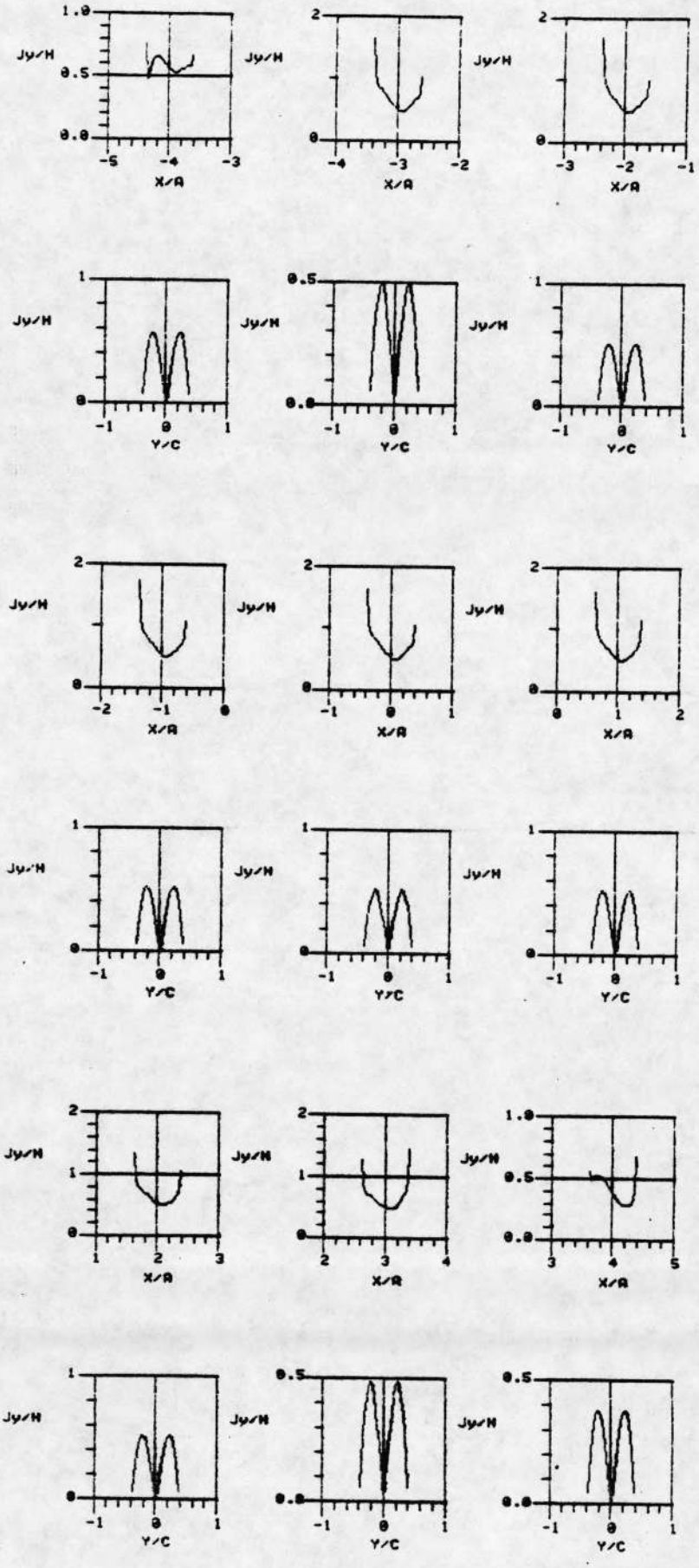

Figure 5(a)

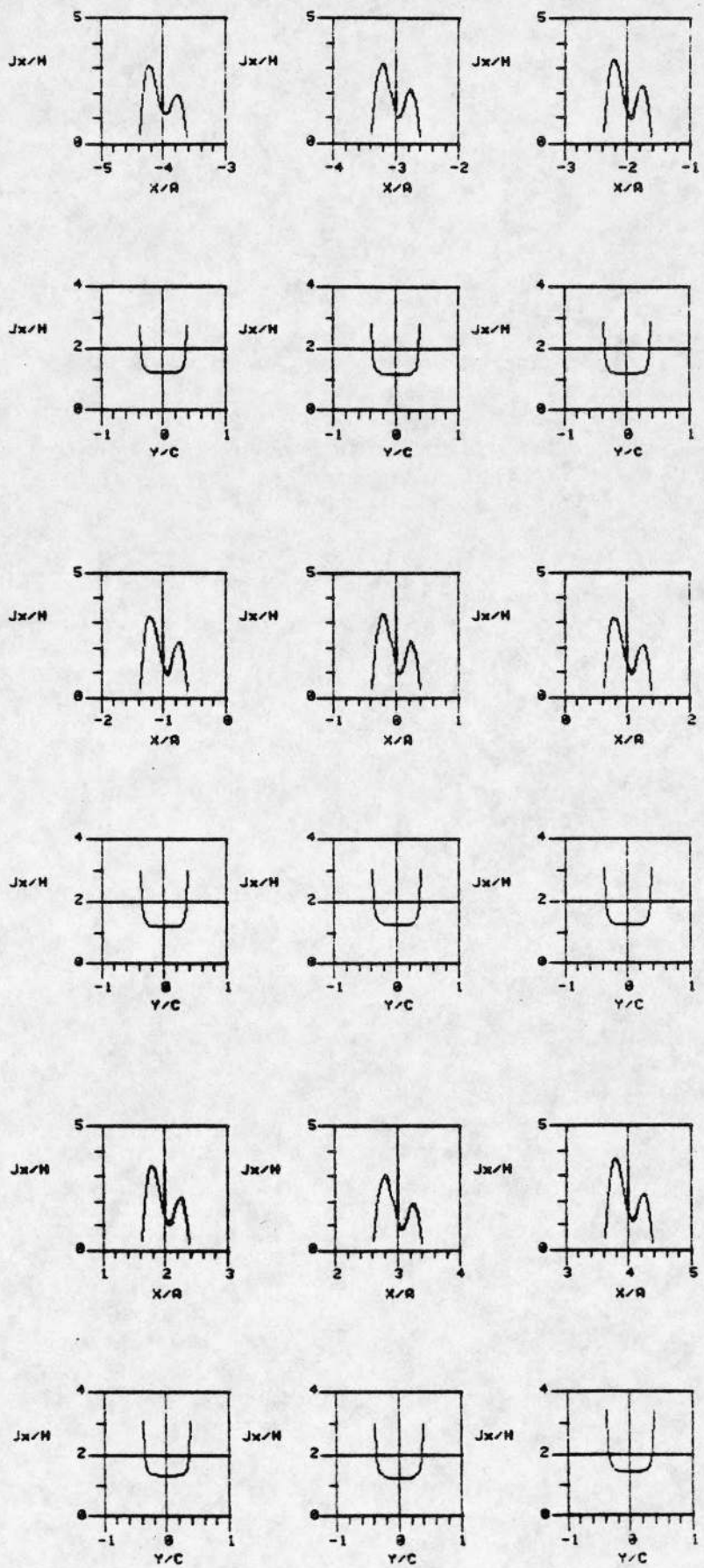

Figure 5(b)

Figure 6. Current distribution on 9 patch finite FSS (A = 1 cm, C = 1 cm, B = 0.8 cm, D = 0.8 cm) for $\theta^i = 45°$ and $\phi^i = 0°$ and TM polarization. Frequency f = 45 GHz.

(a) $J_y/|H^i|$ vs. x sampled at y = -d/4, and $J_y/|H^i|$ vs. y sampled at center line of each patch.

(b) $J_x/|H^i|$ vs. x and y sampled at center lines of each patch in the horizonal and vertical directions.

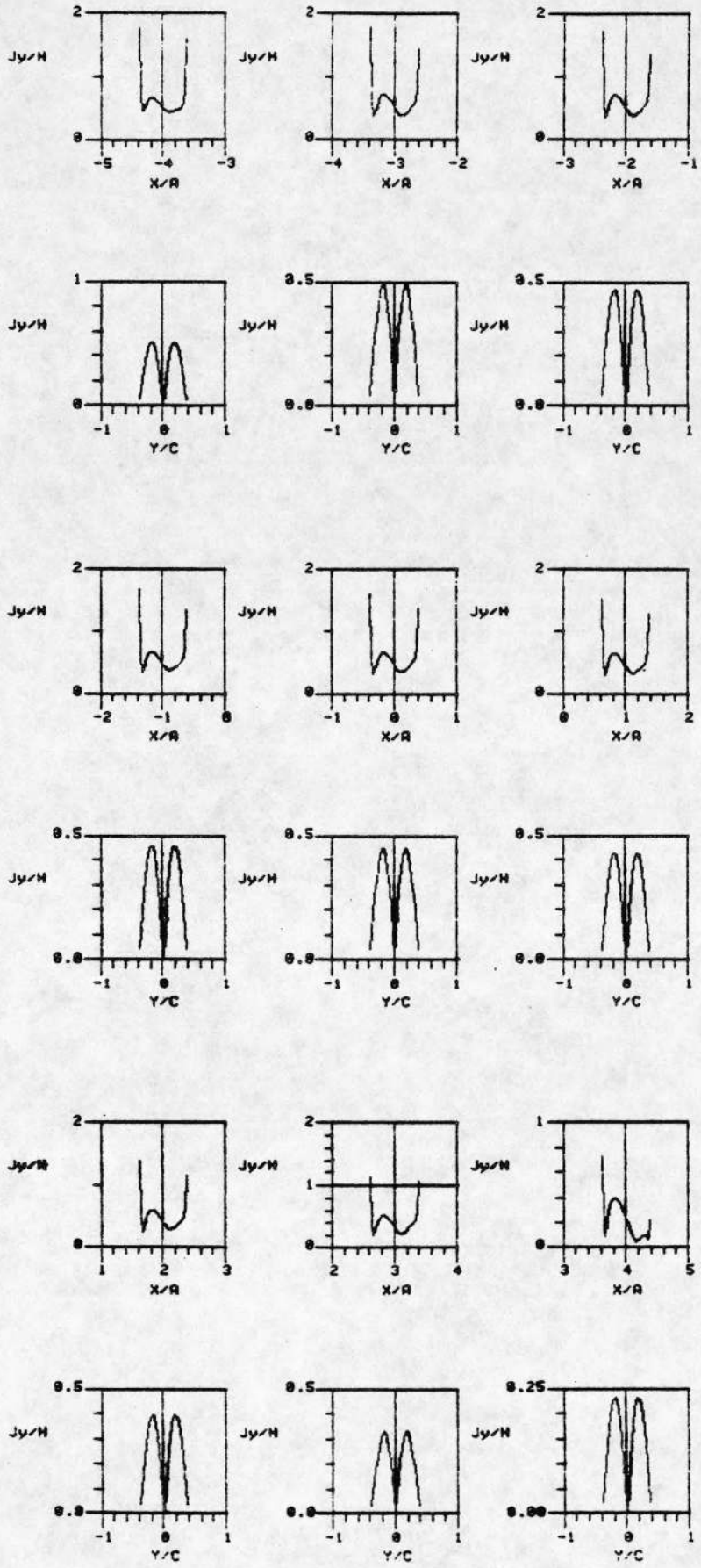

Figure 6(a)

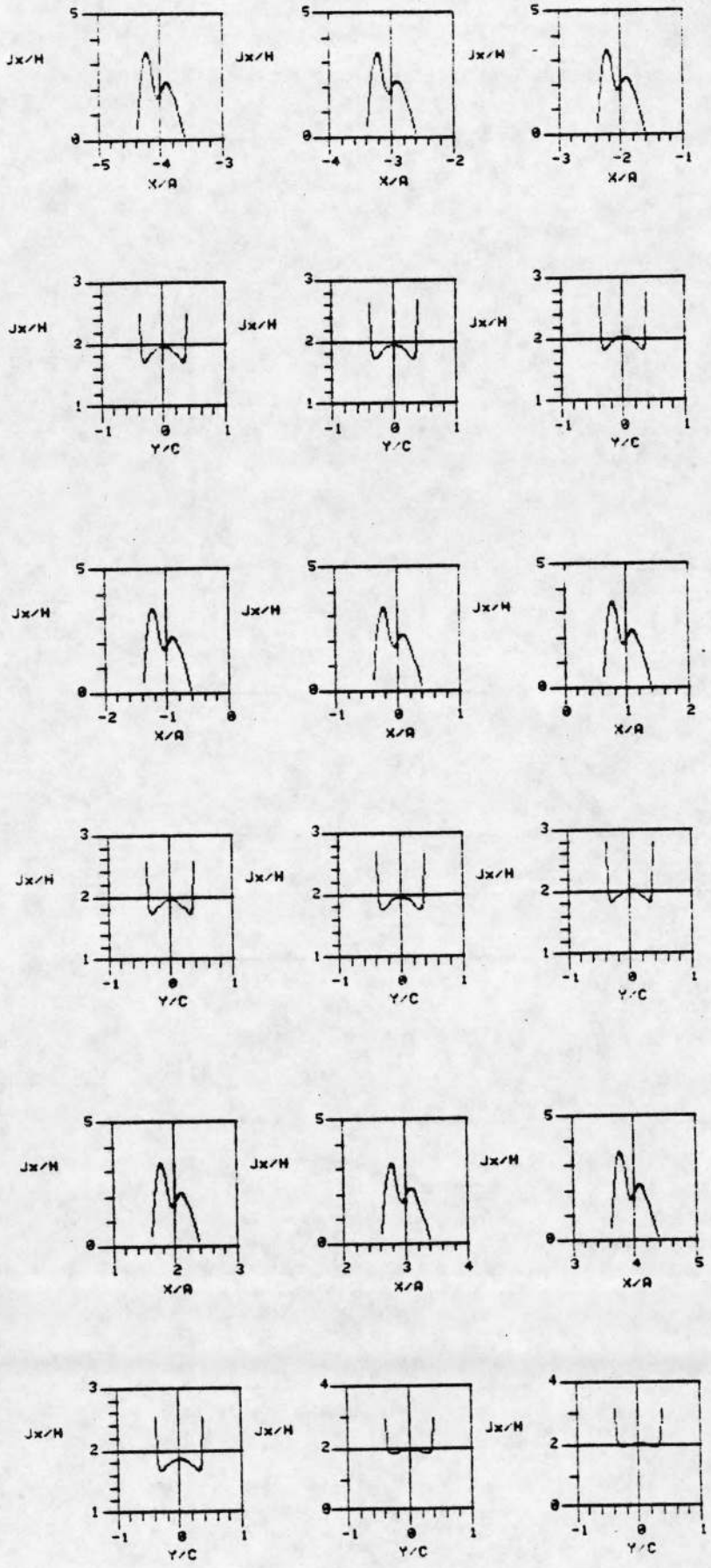

Figure 6(b)

Figure 7. Current distribution on 5 patch finite FSS (A = 1 cm, C = 1 cm, B = 0.8 cm, D = 0.8 cm) for $\theta^i = 45°$ and $\phi^i = 0°$ and TM polarization. Frequency f = 24 GHz.

(a) $J_y/|H^i|$ vs. x sampled at y = -d/4, and $J_y/|H^i|$ vs. y sampled at center line of each patch.

(b) $J_x/|H^i|$ vs. x and y sampled at center lines of each patch in the horizonal and vertical directions.

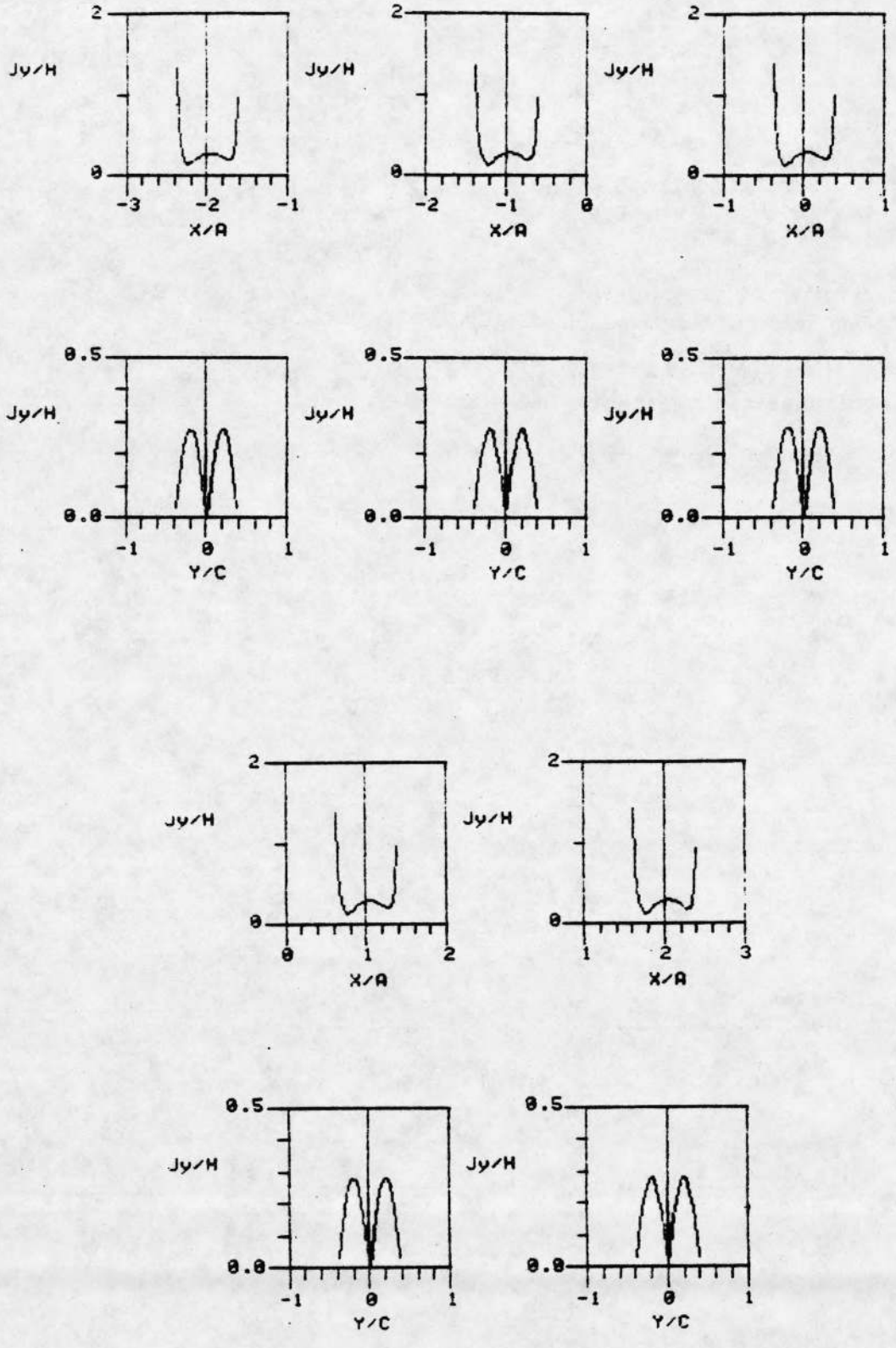
Jy/H
2
0
-3
-2
-1
X/A
Jy/H
2
0
-2
-1
0
X/A
Jy/H
2
0
-1
0
1
X/A
Jy/H
0.5
0.0
-1
0
1
Y/C
Jy/H
0.5
0.0
-1
0
1
Y/C
Jy/H
0.5
0.0
-1
0
1
Y/C
Jy/H
2
0
0
1
2
X/A
Jy/H
2
0
1
2
3
X/A
Jy/H
0.5
0.0
-1
0
1
Y/C
Jy/H
0.5
0.0
-1
0
1
Y/C

Figure 7(a)

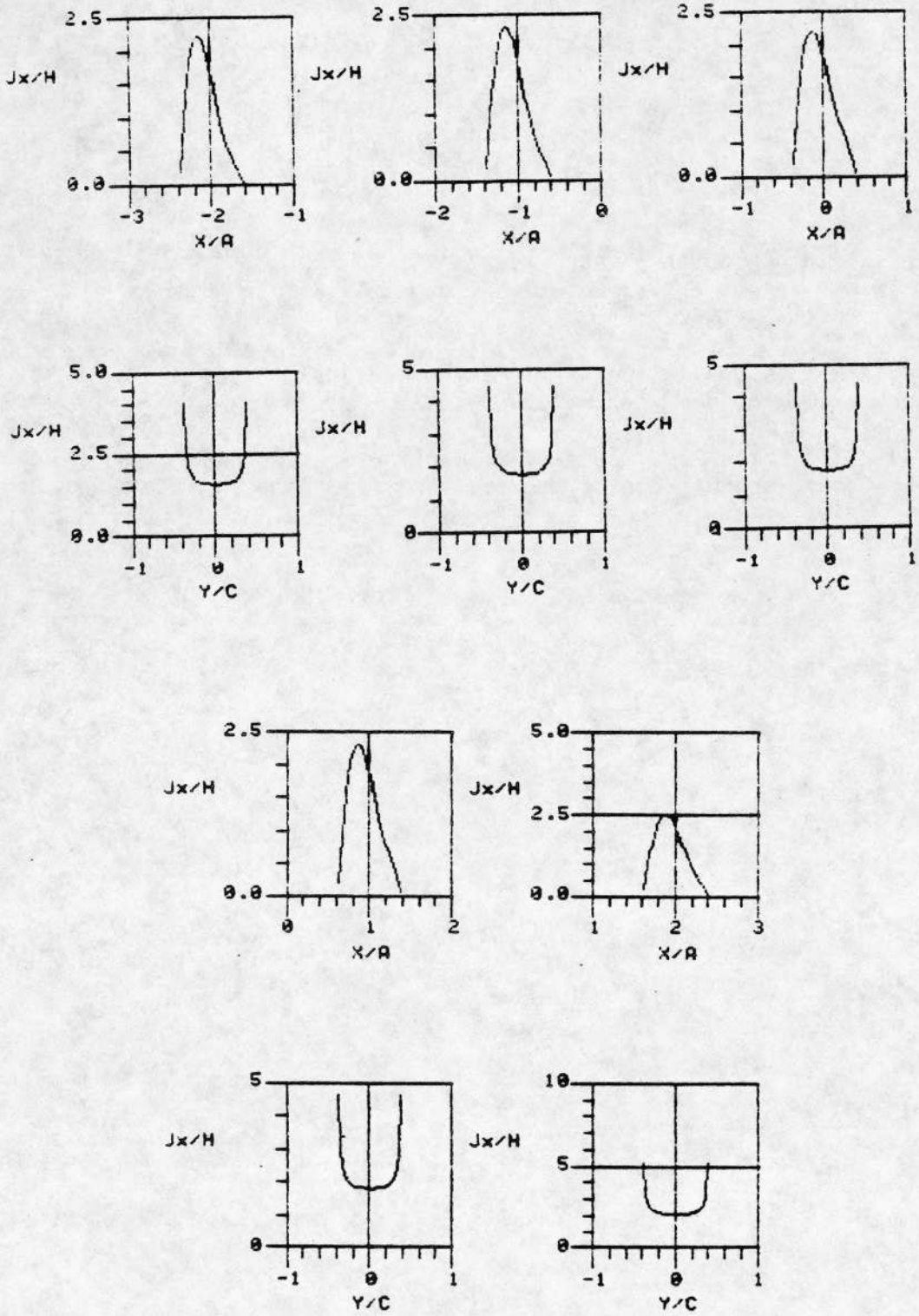

Figure 7(b)

Figure 8. Current distribution on 3 patch finite FSS (A = 1 cm, C = 1 cm, B = 0.8 cm, D = 0.8 cm) for $\theta^i = 45°$ and $\phi^i = 0°$ and TM polarization. Frequency f = 24 GHz.

(a) $J_y/|H^i|$ vs. x sampled at y = -d/4, and $J_y/|H^i|$ vs. y sampled at center line of each patch.

(b) $J_x/|H^i|$ vs. x and y sampled at center lines of each patch in the horizonal and vertical directions.

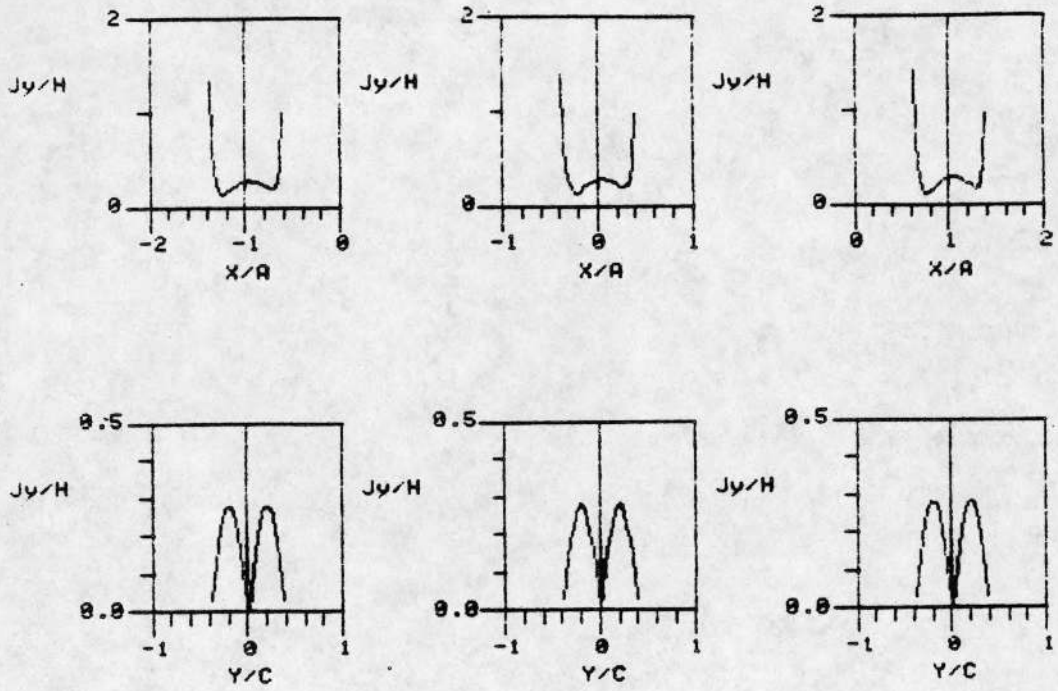

Figure 8(a)

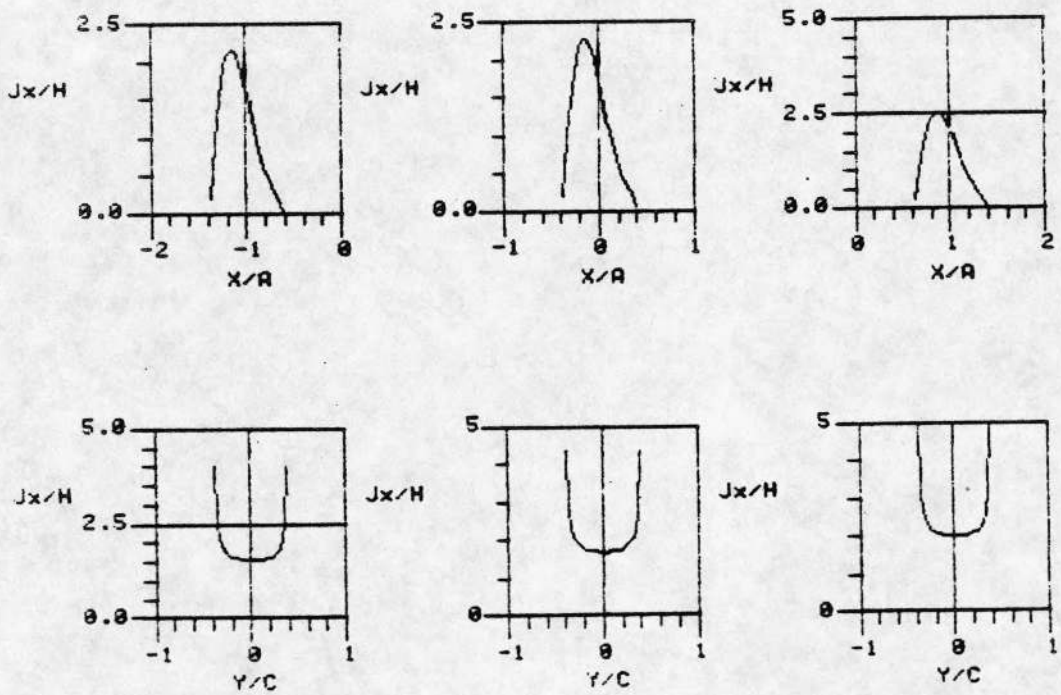

Figure 8(b)

Figure 9. Current distribution on 3 patch finite FSS (A = 1 cm, C = 1 cm, B = 0.8 cm, D = 0.8 cm) for $\theta^i = 0°$ and $\phi^i = 0°$ and TM polarization. Frequency f = 24 GHz.

(a) $J_y/|H^i|$ vs. x sampled at y = -d/4, and $J_y/|H^i|$ vs. y sampled at center line of each patch.

(b) $J_x/|H^i|$ vs. x and y sampled at center lines of each patch in the horizonal and vertical directions.

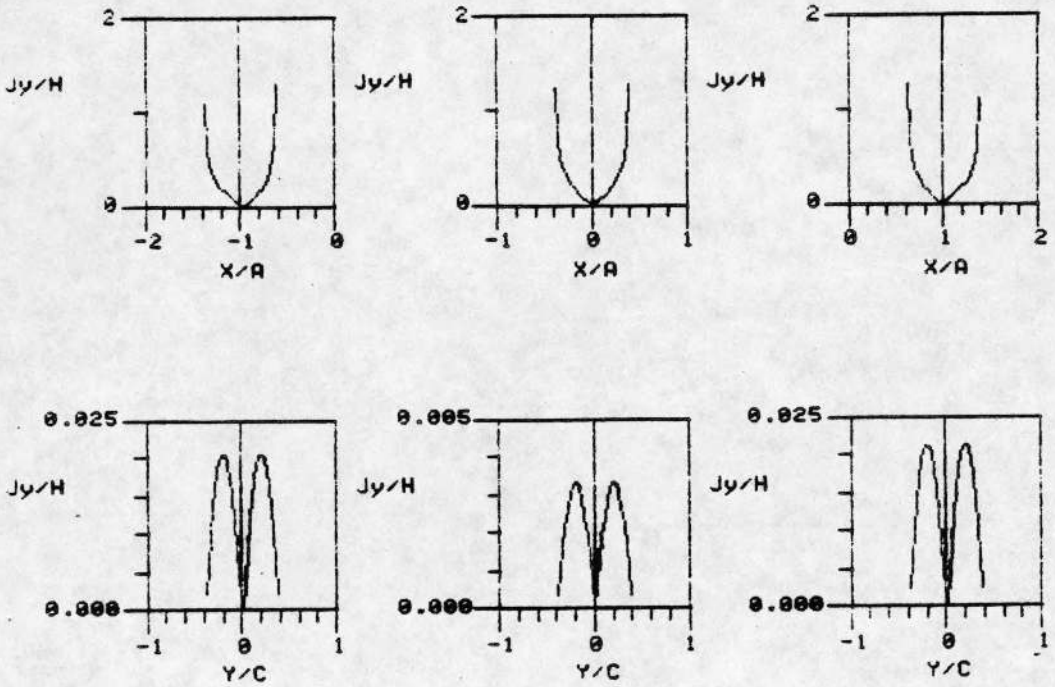

Figure 9(a)

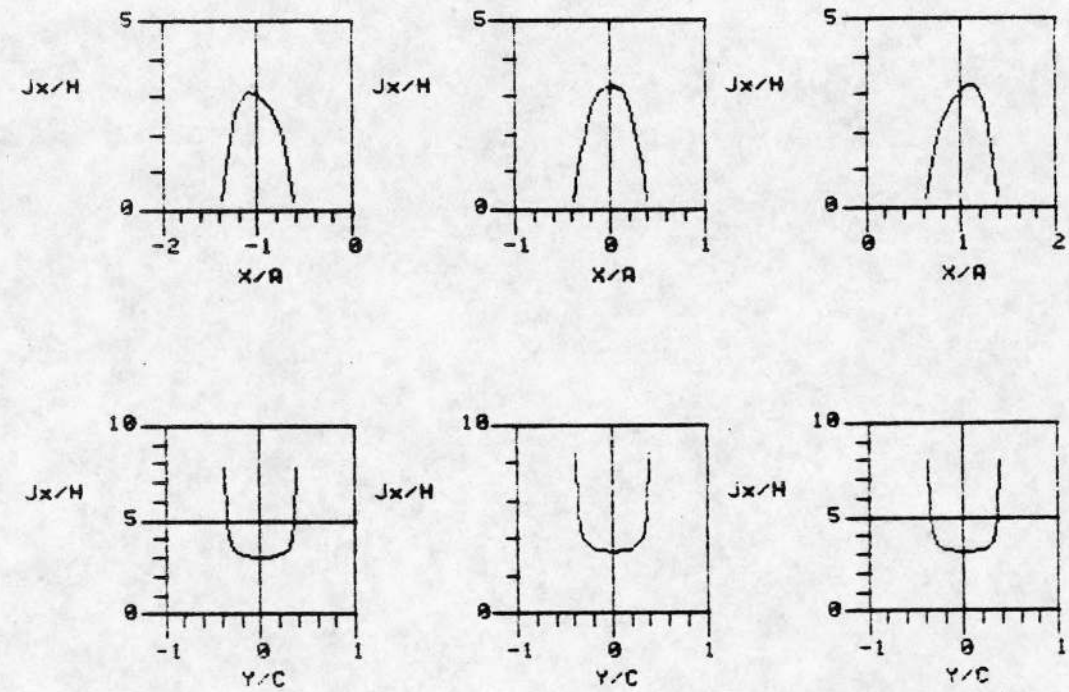

Figure 9(b)

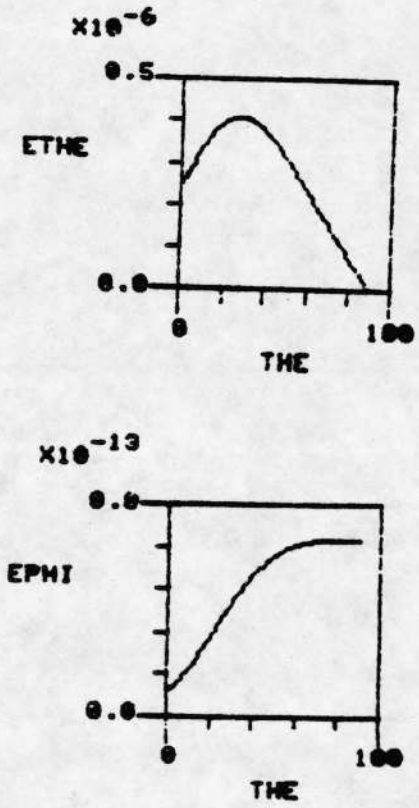

Figure 10. Co-polarized and cross-polarized far-field components, E_θ and E_ϕ. Parameters same as in Fig. 2.

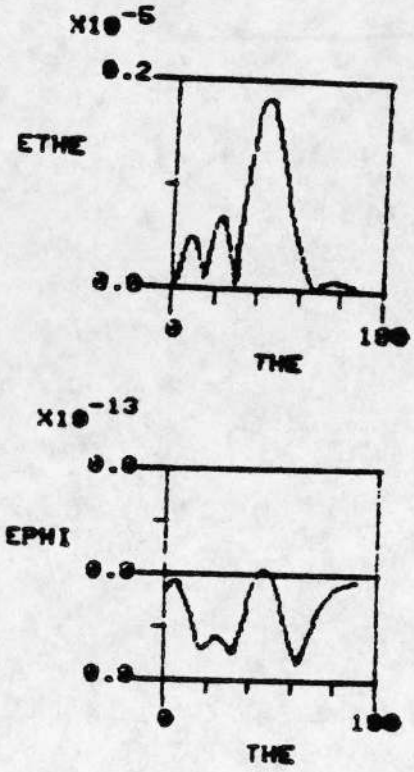

Figure 11. Co-polarized and cross-polarized far-field components, E_θ and E_ϕ. Parameters same as in Fig. 3.

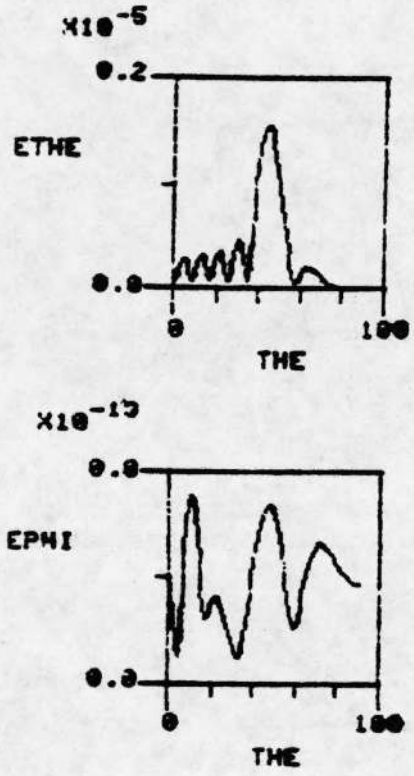

Figure 12. Co-polarized and cross-polarized far-field components, E_θ and E_ϕ. Parameters same as in Fig. 4.

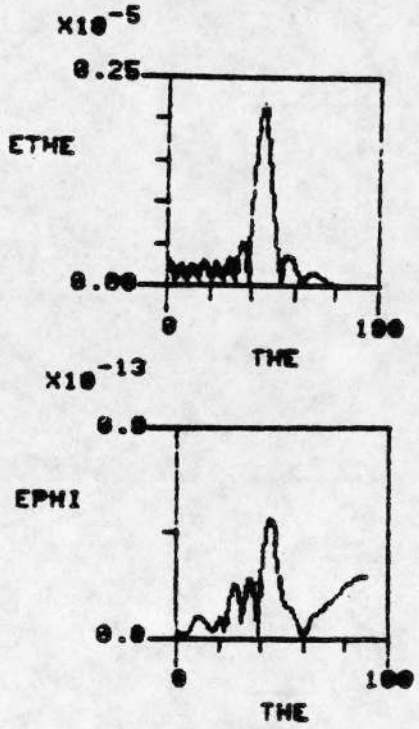

Figure 13. Co-polarized and cross-polarized far-field components, E_θ and E_ϕ. Parameters same as in Fig. 5.

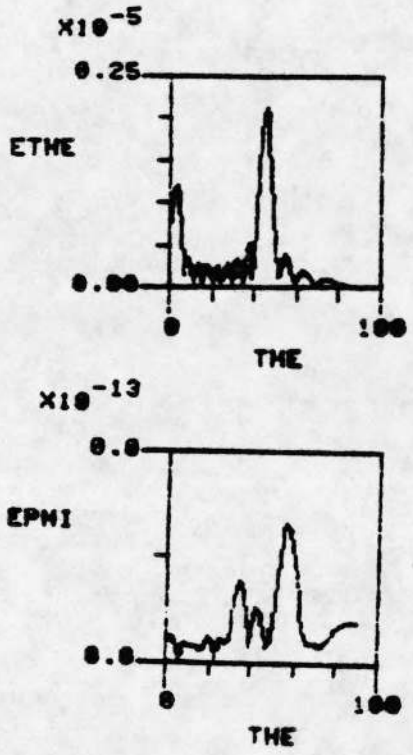

Figure 14. Co-polarized and cross-polarized far-field components, E_θ and E_ϕ. Parameters same as in Fig. 6.

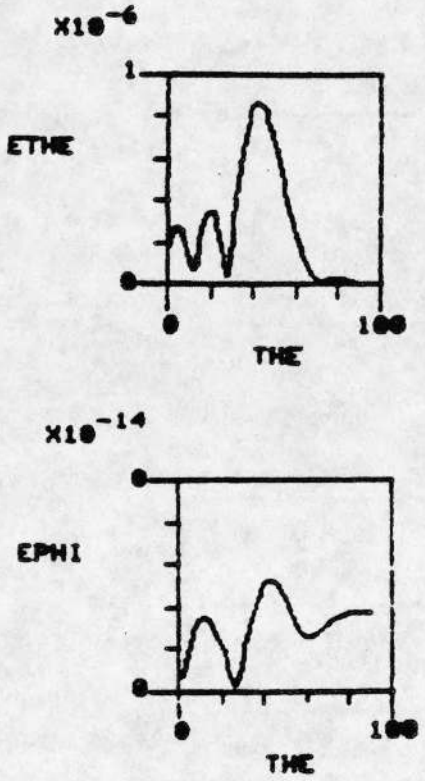

Figure 15. Co-polarized and cross-polarized far-field components, E_θ and E_ϕ. Parameters same as in Fig. 7.

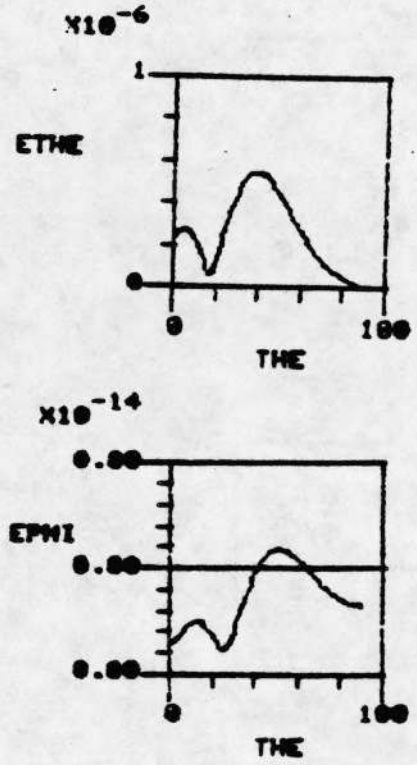

Figure 16. Co-polarized and cross-polarized far-field components, E_θ and E_ϕ. Parameters same as in Fig. 8.

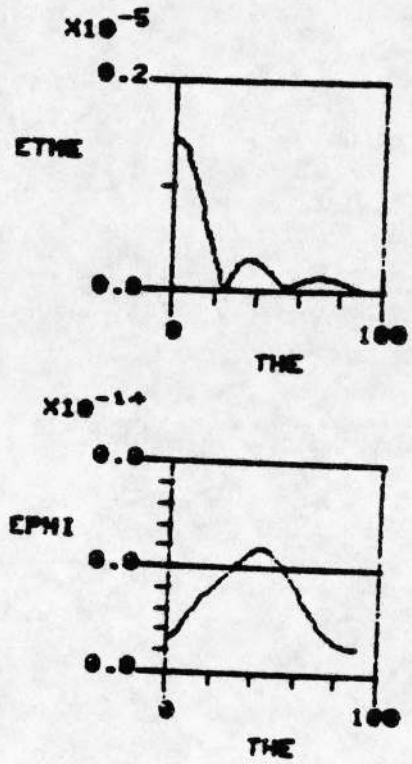

Figure 17. Co-polarized and cross-polarized far-field components, E_θ and E_ϕ. Parameters same as in Fig. 9.